Optimising probe holder design for sentinel lymph node imaging using clinical photoacoustic system with Monte Carlo simulation

Sivasubramanian, Kathyayini; Periyasamy, Vijitha; Wen, Kew Kok; Pramanik, Manojit

2017

Sivasubramanian, K., Periyasamy, V., Wen, K. K., & Pramanik, M. (2017). Optimising probe holder design for sentinel lymph node imaging using clinical photoacoustic system with Monte Carlo simulation. Proceeding of SPIE 10064, Photons Plus Ultrasound: Imaging and Sensing 2017, 100645N-.

https://hdl.handle.net/10356/80359

https://doi.org/10.1117/12.2250478

Optimising probe holder design for sentinel lymph node imaging using clinical photoacoustic system with Monte Carlo simulation

Kathyayini Sivasubramanian, Vijitha Periyasamy, Kew Kok Wen, and Manojit Pramanik[1]
School of Chemical and Biomedical Engineering, Nanyang Technological University, Singapore 637459

ABSTRACT

Photoacoustic tomography is a hybrid imaging modality that combines optical and ultrasound imaging. It is rapidly gaining attention in the field of medical imaging. The challenge is to translate it into a clinical setup. In this work, we report the development of a handheld clinical photoacoustic imaging system. A clinical ultrasound imaging system is modified to integrate photoacoustic imaging with the ultrasound imaging. Hence, light delivery has been integrated with the ultrasound probe. The angle of light delivery is optimized in this work with respect to the depth of imaging. Optimization was performed based on Monte Carlo simulation for light transport in tissues. Based on the simulation results, the probe holders were fabricated using 3D printing. Similar results were obtained experimentally using phantoms. Phantoms were developed to mimic sentinel lymph node imaging scenario. Also, *in vivo* sentinel lymph node imaging was done using the same system with contrast agent methylene blue up to a depth of 1.5 cm. The results validate that one can use Monte Carlo simulation as a tool to optimize the probe holder design depending on the imaging needs. This eliminates a trial and error approach generally used for designing a probe holder.

Keywords: Photoacoustic tomography, Handheld probe, Clinical photoacoustic system, Monte Carlo simulations, Sentinel lymph node imaging.

1. INTRODUCTION

Photoacoustic tomography (PAT) is a hybrid imaging modality, gaining importance rapidly in the field of biomedical imaging. It utilizes the high contrast of optical absorption and high resolution of ultrasound imaging.[1-5] It's clinical applications include sentinel lymph node imaging, breast cancer imaging, brain imaging, temperature sensing etc.[6-10] The advantages of PAT in comparison to other optical imaging modalities are many, like deeper penetration depth, good spatial resolution, and high soft tissue contrast. In PAT, a pulsed laser light is used to irradiate the tissue sample. The light is absorbed by the chromophores present in the tissue. Due to thermo-elastic expansion, the absorbed light produces a local temperature rise leading to the generation of the photoacoustic (PA) waves. The PA signals are detected by an ultrasonic transducer placed on the surface of the tissue and are used to image the light absorption map inside the tissue. Blood, melanin, or even water are some of the intrinsic contrast agents. To improve the contrast, several exogenous contrast agents (organic dyes, metal nanoparticles etc.) were developed which can be used for targeted molecular imaging also.[11-15]

With respect to PA signal detection, single element ultrasound transducer based scanners require mechanical scanning and hence slow.[16] Therefore, not suitable in a clinical scenario. So, clinical ultrasound array based transducers are better suited for clinical applications. Therefore, integrating clinical ultrasound system for PA imaging is a better solution for clinical translation.[17] To achieve this one needs to find ways to integrate the light delivery and the ultrasound probe. It can be done by modifying the ultrasound transducer to incorporate the laser light delivery internally. A pulsed laser diode was integrated inside the linear array transducer to develop an integrated photoacoustic ultrasound imaging system (PAUS).[18] However, the energy of the light source is not high enough for deep tissue imaging. The other, more practical approach is to externally integrate the laser light delivery with the ultrasound probe. This method was used for the guided needle biopsy of the sentinel lymph nodes (SLN) for both pre-clinical and clinical imaging.[8, 19]

[1] Email: manojit@ntu.edu.sg

Photons Plus Ultrasound: Imaging and Sensing 2017, edited by Alexander A. Oraevsky, Lihong V. Wang, Proc. of SPIE Vol. 10064, 100645N · © 2017 SPIE · CCC code: 1605-7422/17/$18 · doi: 10.1117/12.2250478

The design of the probe holder may also vary depending on the area/organ being imaged. Here, we focus on sentinel lymph node (SLN) imaging. Noninvasive SLN identification with PA imaging is a promising tool for breast cancer staging.[8, 19] Sentinel lymph node biopsy (SLNB) is commonly used for staging of breast cancer. To visualize the lymph nodes methylene blue dye or radioactive colloids are commonly used. In this work, MCES is used to study the effect of light delivery angle for varying of depths of SLN imaging.[20-22] Monte Carlo code by Wang *et al.*[23] was modified for fiber source illumination and to handle refractive index mismatch of embedded sphere (SLN is modelled as a sphere) and tissue. Before selecting the various parameters different scenarios were simulated to optimize the probe holder design. The effect of fiber-to-probe distance (FPD) was computed for different angles of illumination for a fixed SLN depth. The light hitting the transducer was also considered, which is more realistic. Also, the effect of fiber-to-tissue distance (FTD) for various light launch angles was studied. Lastly, for a fixed FPD and FTD, angle of light illumination was varied at different SLN depths inside the tissue. Simulations and experiments were performed to validate that Monte Carlo simulations can be used as a precursor for optimizing PA imaging.

2. MATERIALS AND METHODS

Monte Carlo simulation for light propagation in multi-layered tissue (MCML) written in ANSI C was modified to embed the SLN inside the tissue layer.[23-25] To simulate light delivery with a bifurcated fiber bundle modifications were done. Each end has 800 fiber tips distributed over a surface of 4 cm x 0.142 cm. The fibers of diameter 200 μm were randomly packed during fabrication. Therefore, to simulate the same, fibers were placed randomly in a rectangular space of 40 mm x 1.42 mm. 2 such sets of 800 fiber tips were distributed to simulate two ends of the bifurcated fiber bundle. The angular distribution of photons exiting the fiber was modeled as a function of its numerical aperture (NA).[26] For achieve angular launch, according to the launching angle the direction cosines of the photons were varied. To optimize the fiber holder design different scenarios were simulated by varying the FPD, FTD, angle of illumination and depth of imaging.

In this work, equal numbers of photons were launched from each fiber tip. Total absorbance in the sphere and distribution of absorbance in 3-dimensional XYZ grids were recorded. PA signal generated is usually directly proportional to the absorbance in the sphere. MATLAB (MathWorks, Massachusetts, USA) was used for generation of the absorption maps. Simulations were run for 16 million photons (10000 photons from each fiber tip). The thickness of the tissue layer above the sphere was varied from 0.5 cm to 3.0 cm in steps of 0.5 cm. In experimental case as the surface of the fiber is stainless steel and the colour of the ultrasound transducer leads to reflection of the diffuse reflected photons from tissue back into the tissue. It is considered that 36% of the diffused reflected photons are diverted back into the medium. This reflection of photons in simulation occurs at the Z = 0 plane. All simulations were done in a desktop computer with an Intel Xeon 3.7 GHz, 64-bit processor, and 16 GB RAM running windows 10 operating system.

The block diagram of the PAT experimental set up is shown in Fig. 1 (a). ECUBE 12R (Alpinion, South Korea) clinical research ultrasound system was used for this study. The excitation soured was an OPO (Continuum, Surelite OPO) laser pumped by a frequency doubled nanosecond pulsed Nd:YAG pump laser (Continuum, Surelite Ex). It generates 5 ns duration pulses at 10 Hz repetition rate with wavelengths tunable from 670 nm to 2500 nm. For the experiments the laser was tuned to 675 nm (absorption of methylene blue). The laser light was coupled to the sample through a one meter long optical fiber bundle (Ceramoptec GmbH, Germany) containing 1600 fused multimode fibers. The fiber bundle was bifurcated towards the end. The two ends of the fiber bundle is fixed in the probe holder designed along with the ultrasound transducer as shown in Fig. 1(c), leading to a handheld system. The coupling efficiency of the fiber was ~65%. The fluence on the sample surface was calculated to be ~6.4 mJ/cm^2. Thus, falling within the ANSI safety limit of 20 mJ/cm^2.[27] The 3D design of the optical bundle holder was done using a computer-aided design (CAD) software. The angles were chosen keeping in mind the limitations caused by the flexibility of the fiber and its length. The fiber holder was designed with two slots to hold two ends of the fiber and a single slot to accommodate the ultrasound transducer. The holder was designed for different angles of light launch from the fiber bundle. The various angles used for the experiments are 0°, 5°, 10°, and 15°. The various probe holders are shown in Fig. 1(b).

Imaging with phantoms mimicking SLN was performed. A linear array transducer L3-12 was used to acquire the PA signal generated from the sample. A spherically shaped transparent object was prepared with latex material of and filled with methylene blue (10 mg/mL). The spherical phantom was embedded in a 3 cm thick chicken breast tissue as shown in Fig. 1(d). For imaging at various depths chicken tissue was sliced at 0.5 cm thickness. They were stacked on top to

increase the depth of imaging from 0.5 cm to 2.5 cm in steps of 0.5 cm. The SLN phantom was placed in water bath on which the handheld probe was placed to acquire PA images at different depths and at different angles of the light launch at FTD 3 cm. The different angles used for light delivery are 0°, 5°, 10°, and 15° at different depths of 0.5 cm, 1 cm, 1.5 cm, 2 cm, and 2.5 cm.

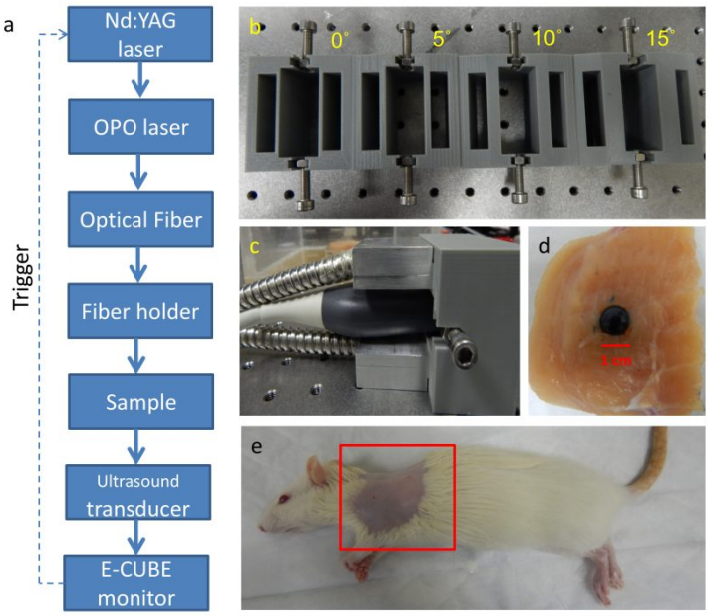

Figure 1: (a) Box diagram showing the various components and flow of the experimental set-up; (b) Photograph showing the 3-D printed fiber holders at various angles of 0°, 5°, 10° and 15°; (c) Photograph of the fiber holder with the two ends of the optical fiber bundles and the linear array ultrasound transducer; (d) image showing the spherical methylene blue phantom embedded in chicken tissue; (e) Photograph of the rat with hair removed in the highlighted area for SLN imaging.

Based on the simulations and phantom experiments best angle was chosen for *in vivo* SLN imaging in rats at a depth of 1 cm by adding chicken tissue (mimic human scenario). Animal experiments were performed according to the approved guidelines and regulations by the institutional Animal Care and Use committee of Nanyang Technological University, Singapore (Animal Protocol Number ARF-SBS/NIE-A0263). Adult Sprague Dawley rats with body weights (200 - 250 g) were used for experiments. Initial anesthesia was done using a mixture of ketamine (85 mg/kg) and xylazine (15 mg/kg). The hair on the region of interest of the rat was gently removed before imaging, using a commercial hair-removal lotion as shown in Fig. 1(e). Intradermal injection of 0.1 mL of MB was performed on a left/right forepaw pad, depending on the side being imaged. Photoacoustic images were acquired after the administration of MB dye. During the data acquisition, anesthesia was maintained using vaporized isoflurane (1 L/min oxygen and 0.75% isoflurane), and a pulse oximeter was used to monitor the vitals. After image acquisition, the animal was euthanized by pentobarbital overdose.

3. RESULTS AND DISCUSSIONS

Monte Carlo simulations were carried out to optimize the light delivery to the SLN as described. The mean (standard deviation) spot size from each fiber bundle is 4.4 (0.58) cm and 0.6 (0.001) cm along X and Y axis, respectively. After optimizing the parameters like FPD, FTD simulation was done to see the effect of different illumination angles at different depths of the SLN. This study was also experimentally validated for SLN (spheres) at different depths. FPD was chosen as approximately 2 cm depending on the bundle holder fabricated. Owing to the limitation of the flexibility of the fiber bundle, maximum possible illumination angle was only 15°. At FTD of 3 cm, we observed maximum absorbance at this angle. Hence, FTD of 3 cm was chosen for both simulations and experiments in this study. Fig. 2 (a) shows the absorbance plot (spheres placed at depth 0.5 cm to 3 cm) for illumination angles 0°, 5°, 10°, and 15°. For spheres at depths (0.5 cm and 1 cm) illumination of 15° gave the maximum absorbance. 10° gave the maximum

absorbance for other depths. Trend in the plots reveal that the angle of launch plays an important role for delivering light from different distances between the fiber-probe and fiber-tissue. With increase in the angle of illumination, propagation of photons towards the center of the geometry (closer to the origin) increases the light absorbance in the sphere. The variation across maximum and minimum absorbance in sphere across angles 0˚ to 15˚ in steps of 5˚ for depths up to 2 cm was more than 50%. Fig. 2 (b-e) shows the light absorption maps in the SLN at depth 1 cm. 320 million photons were simulated for obtaining the smooth absorption maps.

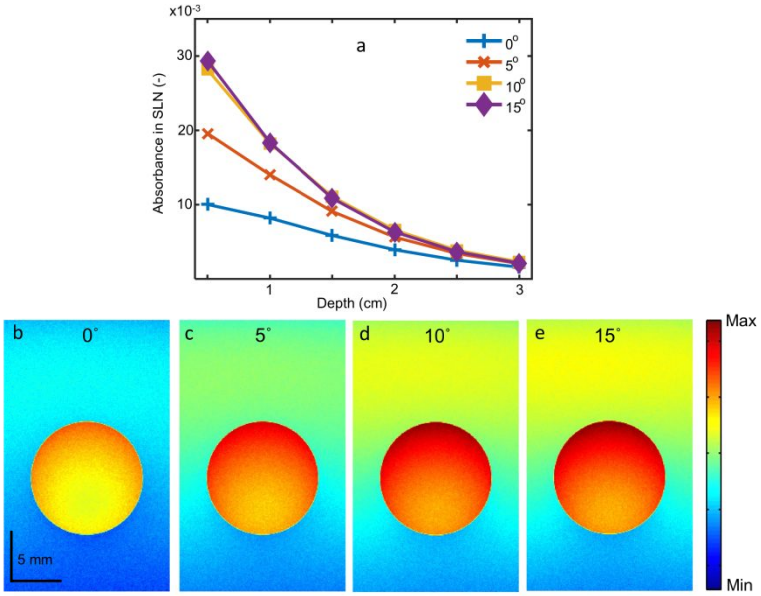

Figure 2: Simulation results. (a) Graph showing the absorbance in the sphere vs depth for angles of illumination of 0˚, 5˚, 10˚ and 15˚ at FPD of ~2 cm and FTD of 3 cm; (b-e) The absorbance maps of sphere at depth 1 cm for illumination angles 0˚, 5˚, 10˚, and 15˚.

Lastly, experiments were done to validate the simulation results. Probe holders were designed to hold the fiber bundle at angles 0°, 5°, 10°, and 15°. Due to the limited length and limited flexibility of the fiber bundle, angle of illumination was limited to 15°. Phantom experiments were carried for various SLN depths of 0.5 cm, 1 cm, 1.5 cm, 2 cm, and 2.5 cm. The fiber to tissue distance was kept at 3 cm. Figure 3(a) shows the signal-to-noise ratio (SNR) obtained from the beam-formed PA images of the SLN phantom using the clinical PA imaging system. $SNR = \frac{V}{n}$, here V is the PA signal amplitude, and n is the standard deviation of the background noise. The SNR is plotted with respect to the depth of the sphere for different angle of illumination.

Trend in the SNR confirms that probe holder design is important depending on the imaging depths and angles of illumination. At 0° the SNR at most of the depths the SNR was the lowest. At lower imaging depths, the variation in SNR was more than 100%. The SNR values do not vary significantly at a depth of 2.5 cm. With increasing depth, the SNR drops irrespective of the angle of launch. From Fig. 3 (a), it is observed that the for depth of 0.5 cm maximum SNR was obtained at an angle of 15°, and for other depths the maximum SNR was obtained at an angle of 10°, which is close match with simulation results. To show the difference, the B-scan PA images of the sphere placed at 1 cm depth only for different angles of illumination is shown in Figures 3 (b-e). Comparing the simulation and the experimental results, it can be concluded that simulation data matches the experimental outcome very closely, as evident from the similar trends in both scenarios. Therefore, Monte Carlo simulation with embedded objects can be used as a precursor to design the probe for various experimental needs.

Based on the simulations and experiments, the angle of illumination of 15°, FTD of 1 cm and FPD of approximately 2 cm were chosen for *in vivo* animal experiments for a depth of 1 cm. From Fig. 4 it can be seen that upon injection of methylene blue the sentinel lymph nodes can be visualized. Also, to confirm this wavelength range was varied from 670 to 870 nm. Fig. 4(a) shows the US and PA overlay image showing strong PA signal from the SLN of the rat at 670 nm,

Fig. 4 (b) US and PA overlay image showing the absence of PA signal from the SLN of the rat at 800 nm. It can be noted that the SLN could not be imaged with the increase in wavelength (peak absorption of MB is at 668 nm). After euthanizing the animal the skin was removed and the SLN filled with MB can be seen with naked eyes as shown in Fig 4(c). The SLN was excised and the size was measured as shown in Fig. 4(d).

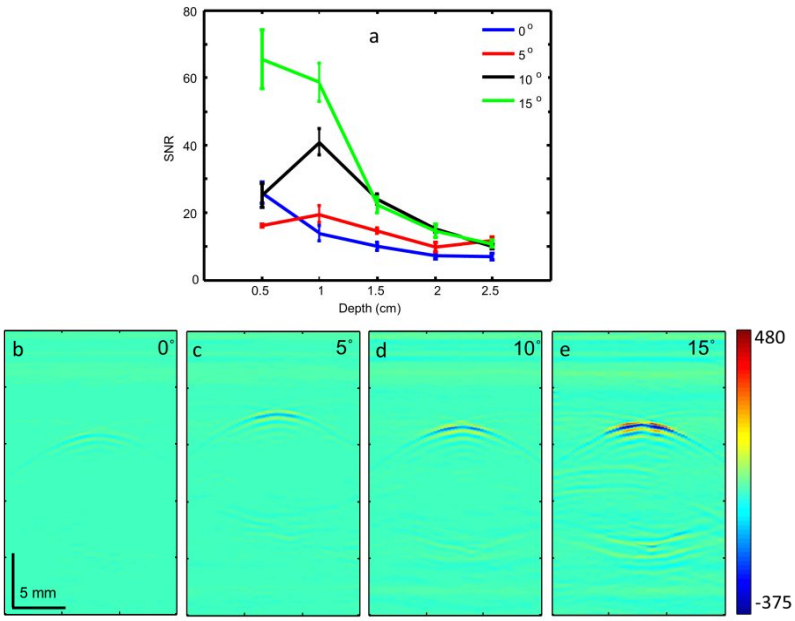

Figure 3: Experimental results. (a) Plot showing the SNR of the PA images for various depths of the SLN for different light launching angles of 0˚, 5˚, 10˚, and 15˚ at FTD of 3 cm; (b-e) B-scan PA images of the spherical MB phantom placed at a depth of 1 cm for various light delivery angles with common colorbar.

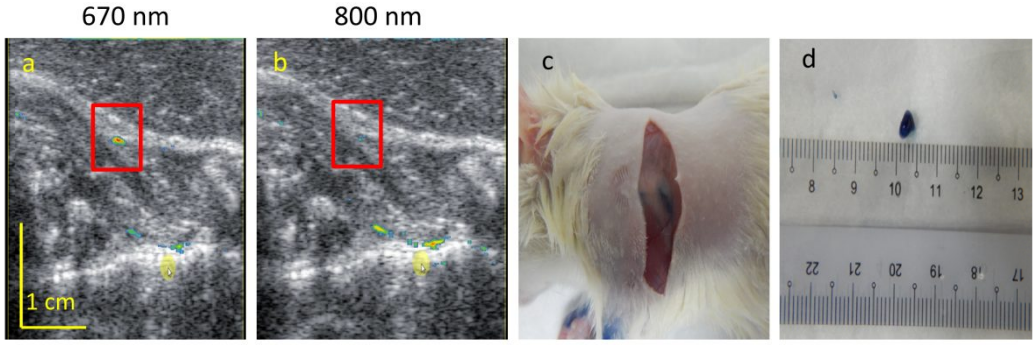

Figure 4: *In vivo* results. (a) US and PA overlay image showing strong PA signal from the SLN of the rat at 670 nm; (b) US and PA overlay image showing the absence of PA signal from the SLN of the rat at 800 nm; (c) Photograph of the imaging area when the outer skin is excised to visualize the SLN filled with MB; (d) Image of the excised SLN form the rat with a scale bar.

There are several factors to be taken into consideration like the angle of illumination, the distance between the transducer and the fiber tip, the distance between the fiber and the skin surface, the depth of the object, etc., which can affect the PA signal. All these parameters were considered for simulation studies, experimentally it was validated only for different light illumination angle with respect to depth at a fixed fiber tissue distance due to practical limitations of the fiber bundle. The imaging setup (target, tissue properties etc.) will also play a key role. Depending on application, there will be different types of tissue, the shape of the target object might be different. Here, we have taken the SLN as a sphere. Another factor that can vary is the light wavelength. Since, methylene blue was used as contrast agent for the SLN

mapping, the excitation wavelength of 675 nm was used. This has to be modified depending on the contrast agent of interest.

4. CONCLUSION

Monte Carlo simulations were done to study the effect of the light launching angles on PA signal using a handheld photoacoustic probe. Different simulation scenarios were considered taking into account the different parameters that will affect the imaging. Experimental validation was provided for the different illumination angles at various SLN depths. It was evident from simulations that illumination angle needs to be varied to obtain maximum absorbance in SLN. Different 3D printed probe holders were designed and PA imaging was done using the clinical ultrasound system. It was reaffirmed through experiments that the angle of light delivery plays an important role with respect to the depth of imaging. From the results the best scenario for *in vivo* imaging was determined. SLN was imaged non-invasively *in vivo* in rats using methylene blue as contrast agents using the handheld probe. Non-invasive needle biopsy of SLN using handheld probe will be part of our future work.

ACKNOWLEDGEMENTS

The authors would like to acknowledge the financial support from the Tier 1 research grant funded by the Ministry of Education in Singapore [RG41/14: M4011285)] and Tier 2 research grant funded by Ministry of Education in Singapore (ARC2/15: M4020238). Authors have no relevant financial interests in the manuscript and no other potential conflicts of interest to disclose.

REFERENCES

[1] Taruttis, A., and Ntziachristos, V., "Advances in real-time multispectral optoacoustic imaging and its applications," Nature Photonics, 9(4), 219-227 (2015).
[2] Wang, L. V., and Hu, S., "Photoacoustic Tomography: In Vivo Imaging from Organelles to Organs," Science, 335(6075), 1458-1462 (2012).
[3] Beard, P., "Biomedical photoacoustic imaging," Interface Focus, 1(4), 602-31 (2011).
[4] Upputuri, P. K., and Pramanik, M., "Recent advances toward preclinical and clinical translation of photoacoustic tomography: a review," Journal of Biomedical Optics, 22(4), 041006 (2017).
[5] Upputuri, P. K., Sivasubramanian, K., Mark, C. S. K. *et al.*, "Recent Developments in Vascular Imaging Techniques in Tissue Engineering and Regenerative Medicine," BioMed Research International, 2015, 9 (2015).
[6] Li, R., Wang, P., Lan, L. *et al.*, "Assessing breast tumor margin by multispectral photoacoustic tomography," Biomedical Optics Express, 6(4), 1273-81 (2015).
[7] Anastasio, M., Mitsuhashi, K., Huang, C. *et al.*, "Recent advancement in transcranial brain imaging using photoacoustic computed tomography," The Journal of the Acoustical Society of America, 135(4), 2208-2208 (2014).
[8] Erpelding, T. N., Kim, C., Pramanik, M. *et al.*, "Sentinel Lymph Nodes in the Rat : Noninvasive Photoacoustic and US imaging with a clinical US system," Radiology, 256(1), 102-110 (2010).
[9] Pramanik, M., and Wang, L. V., "Thermoacoustic and photoacoustic sensing of temperature," Journal of Biomedical Optics, 14(5), 054024 (2009).
[10] Cai, X., Kim, C., Pramanik, M. *et al.*, "Photoacoustic tomography of foreign bodies in soft biological tissue," Journal of Biomedical Optics, 16(4), 046017 (2011).
[11] Sivasubramanian, K., Mathiyazhakan, M., Wiraja, C. *et al.*, "Near Infrared light-responsive liposomal contrast agent for photoacoustic imaging and drug release applications," Journal of Biomedical Optics, 22(4), 041007 (2017).
[12] Lyu, Y., Fang, Y., Miao, Q. *et al.*, "Intraparticle Molecular Orbital Engineering of Semiconducting Polymer Nanoparticles as Amplified Theranostics for in Vivo Photoacoustic Imaging and Photothermal Therapy," ACS Nano, 10(4), 4472-4481 (2016).
[13] Huang, S., Upputuri, P. K., Liu, H. *et al.*, "A dual-functional benzobisthiadiazole derivative as an effective theranostic agent for near-infrared photoacoustic imaging and photothermal therapy," Journal of Materials Chemistry B, 4(9), 1696-1703 (2016).
[14] Kim, C., Favazza, C., and Wang, L. V., "In vivo photoacoustic tomography of chemicals: high-resolution functional and molecular optical imaging at new depths," Chemical Reviews, 110(5), 2756-82 (2010).

[15] Pramanik, M., Song, K. H., Swierczewska, M. *et al.*, "In vivo carbon nanotube-enhanced non-invasive photoacoustic mapping of the sentinel lymph node," Phys Med Biol, 54(11), 3291-3301 (2009).
[16] Upputuri, P. K., and Pramanik, M., "Performance characterization of low-cost, high-speed, portable pulsed laser diode photoacoustic tomography (PLD-PAT) system," Biomedical Optics Express, 6(10), 4118-29 (2015).
[17] Sivasubramanian, K., and Pramanik, M., "High frame rate photoacoustic imaging at 7000 frames per second using clinical ultrasound system," Biomedical Optics Express, 7(2), 312-323 (2016).
[18] Daoudi, K., van den Berg, P. J., Rabot, O. *et al.*, "Handheld probe integrating laser diode and ultrasound transducer array for ultrasound/photoacoustic dual modality imaging," Optics Express, 22(21), 26365-74 (2014).
[19] Garcia-Uribe, A., Erpelding, T. N., Krumholz, A. *et al.*, "Dual-Modality Photoacoustic and Ultrasound Imaging System for Noninvasive Sentinel Lymph Node Detection in Patients with Breast Cancer," Scientific Reports, 5, 15748 (2015).
[20] Periyasamy, V., Sil, S., Dhal, G. *et al.*, "Experimentally validated Raman Monte Carlo simulation for a cuboid object to obtain Raman spectroscopic signatures for hidden material," Journal of Raman Spectroscopy, 46(7), 669–676 (2015).
[21] Valentine, R., Wood, K., Brown, C. *et al.*, "Monte Carlo simulations for optimal light delivery in photodynamic therapy of non-melanoma skin cancer," Physics in medicine and biology, 57(20), 6327 (2012).
[22] Liu, Q., Zhu, C., and Ramanujam, N., "Experimental validation of Monte Carlo modeling of fluorescence in tissues in the UV-visible spectrum," Journal of Biomedical Optics, 8(2), 223-236 (2003).
[23] Wang, L. V., Jacques, S. L., and Zheng, L., "MCML - Monte Carlo modeling of light transport in multi-layered tissues," Computer Methods and Programs in Biomedicine, 47(2), 131-146 (1995).
[24] Periyasamy, V., and Pramanik, M., "Monte Carlo simulation of light transport in turbid medium with embedded object—spherical, cylindrical, ellipsoidal, or cuboidal objects embedded within multilayered tissues," Journal of Biomedical Optics, 19(4), 045003 (2014).
[25] Periyasamy, V., and Pramanik, M., "Monte Carlo simulation of light transport in tissue for optimizing light delivery in photoacoustic imaging of the sentinel lymph node," Journal of Biomedical Optics, 18(10), 106008 (2013).
[26] Naglič, P., Pernuš, F., Likar, B. *et al.*, "Limitations of the commonly used simplified laterally uniform optical fiber probe-tissue interface in Monte Carlo simulations of diffuse reflectance," Biomedical Optics Express, 6(10), 3973-3988 (2015).
[27] "American National Standard for Safe Use of Lasers," ANSI Standard Z136.1-2000, NY, (2000).